

Josephson Current in Ballistic Graphene Corbino Disk

Babak Abdollahipour,^{1, a)} Ramin Mohammadkhani,² and Mina Khalilzadeh²

¹⁾Faculty of Physics, University of Tabriz, Tabriz 51666-16471, Iran

²⁾Department of Physics, Faculty of Science, University of Zanjan, Zanjan 45371-38791, Iran

We solve Dirac-Bogoliubov-De-Gennes (DBdG) equation in a superconductor-normal graphene-superconductor (SGS) junction with Corbino disk structure to investigate the Josephson current through this junction. We find that the critical current I_c has a nonzero value at Dirac point in which the concentration of the carriers is zero. We show this nonzero critical current depends on the system geometry and it decreases monotonically to zero by increasing the ratio of the outer to inner radii of the Corbino disk (R_2/R_1), while in the limit of $R_2/R_1 \rightarrow 1$ it scales like a diffusive Corbino disk. The product of the critical current and the normal-state resistance $I_c R_N$ attains the same value for the planar structure at zero doping. These results reveals the pseudodiffusive behavior of the graphene Corbino Josephson junction similar to the planar structure.

PACS numbers: 74.45.+c, 74.50.+r, 73.63.-b, 74.78.Na.

I. INTRODUCTION

A dissipationless current in equilibrium could exist between two superconductors separated by a thin insulating layer and its value would be proportional to the sine of the phase difference of the superconductors order parameters, which is called the Josephson effect¹. Further studies have shown that Josephson effect can exist if superconductors are connected by a weak link (for a review see Ref. 2) in which superconducting correlations can propagate through a weak link material via the process of retro Andreev reflection (AR) at their interfaces³. Conversion of the subgap electron and hole excitations with opposite spin directions to each other by successive retro AR at two interfaces leads to the formation of a supercurrent. The Josephson effect is characterized by the critical current I_c (maximum of the Josephson current) which is characteristic of the strength of weak link and its geometry.

The field of Josephson junctions received new attention recently, after it was recognized that suitable Josephson devices might serve as quantum bits (qubits) in quantum information devices and that quantum logic operations could be performed by controlling gate voltages or magnetic fields^{4,5}. This system is attractive because the low dissipation inherent to superconductors make possible, in principle, long coherence times. In addition, because complex superconducting circuits can be microfabricated using integrated-circuit processing techniques, scaling to a large number of qubits should be relatively straightforward^{6,7}. Further, reading out of a state of superconducting qubit has been realized experimentally by using ballistic Josephson vortices (fluxon)^{8,9}. It is performed by measuring the microwave radiation induced by a fluxon moving in an annular Josephson junction. These studies and experiments motivate us to explore graphene

Josephson junctions with Corbino geometry. Results of this study may be helpful in realizing new type of superconducting qubits or in reading out of their states.

Graphene, a two dimensional single layer of graphite which has been isolated by Novoselov *et al*¹⁰, shows a unique electronic properties due to its peculiar gapless semiconducting band structure¹¹⁻¹³. The conduction and valence bands in graphene touch each other at two inequivalent corners of the hexagonal Brillouin zone in reciprocal space, normally called K and K' points or Dirac points. The dispersion relation of the quasiparticle excitations about these K and K' points is linear and obey Dirac equation (for a review see Ref. 14). The presence of such low-lying excitations leads to unusual properties for graphene including specular Andreev reflection at the interface with a superconductor¹⁵ and Klein tunneling in p - n junctions¹⁶. These important features of graphene has attracted intense theoretical and experimental attention to study the effect of the relativistic-like dynamics of electrons on Josephson effect which are already known in ordinary conducting systems.

In the last several years graphene has become a new class of weak link materials in Josephson junctions. The graphene Josephson junction has been studied theoretically¹⁷⁻²⁴ and experimentally²⁵⁻³⁰. Titov and Beenakker have considered a planar structure in which two superconductors are connected to each other via an undoped strip of ballistic graphene¹⁷. Using Dirac-Bogoliubov-de Gennes equation¹⁵, they have shown that a nonzero supercurrent can flow through a ballistic Josephson junction even at the Dirac point in which the carriers concentration is zero. They have found that the critical current I_c for a wide graphene junction at the Dirac point has the same form as in an ordinary disordered normal metal³¹. The Josephson effect has been studied in the graphene nanoribbons of length L smaller than superconducting coherence length and arbitrary width W with smooth, armchair and zigzag edges by Moghaddam and Zareyan^{18,19}. They have obtained that in contrast to an ordinary superconducting

^{a)}Electronic mail: b-abdollahi@tabrizu.ac.ir

quantum point contact (SQPC) the supercurrent I_c in smooth and armchair ribbons with a low concentration of the carriers is not quantized but decreases monotonically by decreasing W/L . At higher concentrations of the carriers this monotonic variation acquires a series of peaks with distances inversely proportional to the chemical potential μ . The phase, the temperature and the junction length dependence of the supercurrent for ballistic graphene Josephson-junctions have been studied by Hagymási *et.al.*²⁰. Black-Schaffer and Doniach have used a tight-binding Bogoliubov-de Gennes (BdG) formalism to self-consistently calculate the proximity effect, Josephson current, and local density of states in ballistic graphene Josephson junctions²¹. They have shown that self-consistency does not notably change the current-phase relationship (CPR) derived earlier for short junctions using the non-self consistent Dirac-BdG formalism. The self-consistent temperature dependence of CPR in ballistic graphene Josephson junctions have been studied by Black-Schaffer and Linder²². Moreover, the effect of the strain on the supercurrent in a ballistic graphene Josephson junction have been studied by Alidoust and Linder²³. They have shown the supercurrent at the charge neutrality point can be tuned efficiently by means of mechanical strain. The many-body effects on the critical current in graphene Josephson junction has been investigated by Gonzalez and Perfetto²⁴.

Heersche *et.al.* have experimentally shown that the superconducting correlations can penetrate into the graphene layer via the proximity effect²⁵. They have confirmed the theoretical prediction that a finite supercurrent can flow at zero charge density. Most of the experimental studies of the graphene Josephson Junctions have been limited to the case of diffusive transport through graphene with poorly defined and modest quality graphene-superconductor interfaces²⁶⁻²⁸. Recently, a ballistic graphene Josephson junction with a well defined and transparent interface to the graphene has been developed using Molybdenum Rhenium contacts²⁹. It has been shown that the critical current oscillates with the carrier density due to phase coherent interference of the electrons and holes that carry the supercurrent. Further, direct measurements of the CPR for Josephson junctions with a graphene barrier has been achieved recently by a phase-sensitive SQUID interferometry technique³⁰.

In this paper, we investigate the Josephson current in a superconductor-normal graphene-superconductor (SGS) junction with Corbino disk structure. The SGS junction under study consists of a ballistic graphene ring surrounded by an inner superconducting lead of radius R_1 and an outer superconducting lead of radius R_2 (Fig. 1). The Corbino geometry has advantage over the planar structure specially when a magnetic field is applied to the sample due to the edge absence^{32,33}. Electronic transport in graphene Corbino structures have been studied by investigating various physical properties of these junctions in the normal state such as conductance³⁴, magnetoconductance³⁵,

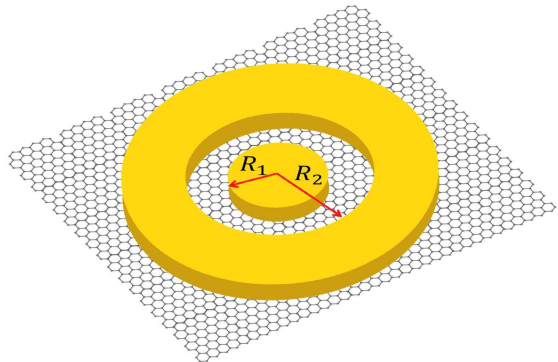


FIG. 1. (Color online) Schematic picture of the graphene Corbino Josephson junction composed of two circular shaped superconducting leads connected via a ballistic graphene ring.

magnetopumping³⁶ and Andreev billiards³⁷. Here, we extend these studies to analyzing of the Josephson current in Corbino structure by solving Dirac-Bogoliubov-de Gennes (DBdG) equation in the polar coordinate and then calculating the Andreev bound states. We show that a critical current can flow through the junction in the limit of zero concentration of the carriers, *i.e.* at Dirac point. Further, we find that the minimal of the critical current depends on the system geometry and reduces as the ratio of the outer to inner radii R_2/R_1 increases.

The paper is organized as follows. In the next section we introduce our model of a ballistic graphene Josephson junction with Corbino disk structure and find the solutions of the DBdG equation in the polar coordinate. Then, we obtain the Josephson current by calculating the Andreev bound states energies. Section III is devoted to presentation of the results and discussions. Finally, we end with a conclusion in Sec. IV.

II. MODEL AND BASIC EQUATIONS

The structure under study is a graphene Corbino Josephson junction composed of a ballistic graphene ring with the inner radius R_1 and the outer radius R_2 connected to two circularly shaped spin singlet superconducting regions, schematically depicted in Fig.1. Superconductivity in graphene is induced via proximity effect by depositing of superconducting electrodes on top of the graphene sheet. We assume that the superconducting regions are heavily doped, such that the Fermi wavelength inside superconducting regions λ_F' is smaller than the Fermi wavelength of graphene λ_F and the superconducting coherence length ξ . Thus we can neglect the suppression of the order parameter $\Delta(\mathbf{r})$ in the superconductors close to the interfaces and we approximate the superconducting order parameter by a step function. Thus, it has constant values $\Delta = \Delta_0 e^{\pm i\phi/2}$ inside superconductors and vanishes identically in normal graphene region¹⁵.

Low energy electron and hole excitations in graphene are described by the Dirac-Bogoliubov-De Gennes (DBdG) equation¹⁵,

$$\begin{pmatrix} \hat{H}_\tau - \mu & \hat{\Delta} \\ \hat{\Delta}^* & \mu - \hat{H}_\tau \end{pmatrix} \Psi = \varepsilon \Psi, \quad (1)$$

where $\Psi = (\psi_e \ \psi_h)^T$ is the four-component wave function in the pseudospin and numbo space, $\hat{\Delta} = \Delta \sigma_0$ is the superconducting pair potential matrix which couples time-reversal electron and hole wave functions ψ_e and ψ_h , $\varepsilon > 0$ denotes the excitation energy measured relative to the chemical potential or the Fermi energy μ . The single-particle Hamiltonian in graphene is the two dimensional Dirac Hamiltonian in each valley $\tau = \pm$, given by

$$\hat{H}_\pm = -i\hbar v(\sigma_x \partial_x \pm \sigma_y \partial_y) + V(r), \quad (2)$$

where, v denotes the Fermi velocity of the quasiparticles in graphene and $\sigma_{i=x,y,z}$ are the Pauli matrices in the sublattice space (pseudospin) with σ_0 representing the 2×2 unit matrix. In the above equation $V(r) = -U_0 \Theta(-r + R_1) \Theta(r - R_2)$ denotes the electrostatic potential throughout the system, which is zero in the normal region and nonzero in the superconductors. Since two valleys are decouple we can solve the Hamiltonian for each valley separately, so we only consider $\hat{H}_+ = \hat{H}$.

To solve DBdG equation in a Corbino disk geometry, we write the Hamiltonian \hat{H} in the polar coordinates (r, φ) as^{37,38},

$$\begin{aligned} \hat{H} = & -i\hbar v(\cos \varphi \sigma_x + \sin \varphi \sigma_y) \partial_x \\ & -i\hbar v(\cos \varphi \sigma_y - \sin \varphi \sigma_x) \frac{1}{r} \partial_\varphi + V(r). \end{aligned} \quad (3)$$

Since the Hamiltonian \hat{H} commutes with the total angular momentum $J_z = l_z + \hbar \sigma_z / 2$, where $l_z = -i\hbar \partial_\varphi$ is the orbital angular momentum in the z direction, its eigenstates ψ are simultaneous eigenstates of J_z . Thus, we can write

$$\Psi = e^{i(m-\frac{1}{2})\varphi} \begin{pmatrix} u_1(\vec{r}) \\ u_2(\vec{r}) e^{i\varphi} \end{pmatrix} \quad (4)$$

where $m = \pm 1/2, \pm 3/2, \dots$, is a half-odd integer corresponding to the angular momentum quantum number. For a constant electrostatic potential wave functions $u_1(\vec{r})$ and $u_2(\vec{r})$ are solutions of the Bessel's differential equation of orders $m - 1/2$ and $m + 1/2$, respectively. Therefore, in the normal region $R_1 < r < R_2$, where $V(r) = \Delta = 0$, the electron and hole like eignstates of the DBdG equation with energy ε are given by,

$$\Psi_N^{e+,-} = e^{i(m-\frac{1}{2})\varphi} \begin{pmatrix} H_{m-\frac{1}{2}}^{(1),(2)}(k_e r) \\ \text{isign}(\mu + \varepsilon) e^{i\varphi} H_{m+\frac{1}{2}}^{(1),(2)}(k_e r) \\ 0 \\ 0 \end{pmatrix} \quad (5)$$

$$\Psi_N^{h-,+} = e^{i(m-\frac{1}{2})\varphi} \begin{pmatrix} 0 \\ 0 \\ H_{m-\frac{1}{2}}^{(1),(2)}(k_h r) \\ \text{isign}(\mu - \varepsilon) e^{i\varphi} H_{m+\frac{1}{2}}^{(1),(2)}(k_h r) \end{pmatrix} \quad (6)$$

where $H_{m-\frac{1}{2}}^{(1),(2)}(k_{e,h} r)$ are Hankel functions of the first and second kinds and $k_{e,(h)} = |\mu + (-)\varepsilon| / (\hbar v)$ denote wave vectors for electrons and holes. In the superconducting leads where the pair potential is $\Delta_{L,R}$, solutions of the DBdG equation are mixed electron-hole excitations. For the inner superconductor ($r < R_1$) the eignstates which are evanescent in this region are given by,

$$\Psi_{S_1}^\pm = e^{i(m-\frac{1}{2})\varphi} \begin{pmatrix} e^{\pm i\beta} H_{m-\frac{1}{2}}^{(1),(2)}(k_\pm r) \\ ie^{\pm i\beta} H_{m+\frac{1}{2}}^{(1),(2)}(k_\pm r) e^{i\varphi} \\ e^{-i\frac{\phi}{2}} H_{m-\frac{1}{2}}^{(1),(2)}(k_\pm r) \\ ie^{-i\frac{\phi}{2}} H_{m+\frac{1}{2}}^{(1),(2)}(k_\pm r) e^{i\varphi} \end{pmatrix}, \quad (7)$$

and for the outer superconductor ($r > R_2$) the evanescent eignstates are,

$$\Psi_{S_2}^\pm = e^{i(m-\frac{1}{2})\varphi} \begin{pmatrix} e^{\mp i\beta} H_{m-\frac{1}{2}}^{(1),(2)}(k_\mp r) \\ ie^{\mp i\beta} H_{m+\frac{1}{2}}^{(1),(2)}(k_\mp r) e^{i\varphi} \\ e^{i\frac{\phi}{2}} H_{m-\frac{1}{2}}^{(1),(2)}(k_\mp r) \\ ie^{i\frac{\phi}{2}} H_{m+\frac{1}{2}}^{(1),(2)}(k_\mp r) e^{i\varphi} \end{pmatrix} \quad (8)$$

where $\beta = \arccos(\varepsilon / \Delta_0)$ and $k_\pm = (\mu + U_0 \pm \sqrt{\varepsilon^2 - \Delta_0^2}) / \hbar v$. The Josephson current through the graphene region is determined by the phase difference ϕ between the superconducting order parameters of two superconductors S_1 and S_2 . This supercurrent is carried by the Andreev bound states, which are formed in the normal graphene region due to the successive conversion of the electron-hole excitations to each other at the normal-superconductor interfaces by Andreev reflection processes. At zero temperature and in the short-junction regime that the separation of the two NS interfaces is small with respect to the superconducting coherence length ξ ($L \ll \xi$), the Andreev bound states (discrete spectrum) with energies $|\varepsilon| \leq \Delta_0$ have the main contribution to the supercurrent. In this limit the Josephson current can be expressed as the following³⁹

$$I(\phi) = -\frac{4e}{\hbar} \frac{d}{d\phi} \int_0^\infty d\varepsilon \sum_{n=0}^\infty \rho_n(\varepsilon, \phi) \varepsilon, \quad (9)$$

where the factor 4 accounts for the spin and valley degeneracies and $\rho_n(\varepsilon, \phi)$ is the density of Andreev bound states. Substitution of $\rho_n(\varepsilon, \phi) = \delta[\varepsilon - \varepsilon_n(\phi)]$, with $\varepsilon_n(\phi)$ denoting the discrete spectrum of the Andreev bound

states, into Eq. (9) gives the supercurrent as,

$$I(\phi) = -\frac{4e}{\hbar} \frac{d}{d\phi} \int_0^\infty d\varepsilon \sum_{n=0}^\infty \delta[\varepsilon - \varepsilon_n(\phi)] \varepsilon$$

$$= -\frac{4e}{\hbar} \sum_{n=0}^\infty \frac{d}{d\phi} \varepsilon_n(\phi) \quad (10)$$

To find the energy spectrum of the Andreev bound states $\varepsilon_n(\phi)$, we follow the approach introduced in Ref.³⁹. Solutions of the wave functions inside the superconductors are rather mixed electron-hole excitations and the interfaces scatter the particles between the two neighboring regions. However, the excited quasiparticles located in the N layer cannot penetrate directly into a superconductor if its energy is smaller than the superconducting pair potential and consequently two kinds of processes, Andreev and normal reflection can occur for them. A simple mode matching at the NS interfaces (namely, $r = R_1$ and $r = R_2$) gives the result for Andreev scattering matrix for the conversion from electron to hole \hat{r}_{he} and \hat{r}_{eh} for that from hole to electron

$$\hat{r}_{he} = e^{-i\beta} \begin{pmatrix} e^{-i\varphi_L} & 0 \\ 0 & e^{-i\varphi_R} \end{pmatrix}, \quad (11)$$

$$\hat{r}_{eh} = e^{-i\beta} \begin{pmatrix} e^{i\varphi_L} & 0 \\ 0 & e^{i\varphi_R} \end{pmatrix}.$$

In obtaining these results we have considered that the Fermi wave length $\lambda_F = \hbar v / (E_F + U_0)$ in S is sufficiently small than the Fermi wave length $\lambda_F = \hbar v / E_F$ in N and the superconducting coherence length $\xi = \hbar v / \Delta_0$. This condition is satisfied simply by taking the limit of $U_0 \rightarrow \infty$. In the normal region the quantum transport of the electron (hole) is described by the scattering matrix $\hat{S}_e(\hat{S}_h)$. The scattering matrices are related to each other by $\hat{S}_h(\varepsilon) = \hat{S}_e(-\varepsilon)^*$. A round trip for the electron or hole wave functions results in a equation for product of the scattering matrices

$$\text{Det} \left(\hat{1} - \hat{r}_{eh} \hat{S}_h \hat{r}_{eh} \hat{S}_e \right) = 0, \quad (12)$$

We can simplify this equation in the short-junction limit $L \ll \xi$ that the length L of the normal region is small relative to the superconducting coherence length, which is experimentally most relevant for superconductors with small gap. In terms of the energy scales this condition is equivalent to $\Delta_0 \ll \hbar / \tau_{dwell} = \hbar v / L$, where τ_{dwell} is the dwell time in the junction. In this regime we may approximate $\hat{S}_{e(h)}(\varepsilon) \simeq \hat{S}_{e(h)}(-\varepsilon) \simeq \hat{S}_{e(h)}(0) \equiv \hat{S}_0^{(*)}$ for ε of order Δ_0 . Using the exact form of the scattering matrix,

$$\hat{S}_0 = \begin{pmatrix} r_{11} & t_{12} \\ t_{21} & r_{22} \end{pmatrix}, \quad (13)$$

and its unitarity $\hat{S}_0^* \hat{S}_0 = \hat{1}$, we can reduce the Eq. 12 to the simpler form of

$$\text{Det} \left[(1 - \varepsilon^2 / \Delta_0^2) \hat{1} - t_{12} t_{12}^\dagger \sin^2(\phi/2) \right] = 0, \quad (14)$$

where $\phi = \phi_R - \phi_L$ is the phase difference between superconductors. We can solve this equation for ε in terms of the eigenvalues of $T = t_{12} t_{12}^\dagger$. Finally, energies of the Andreev bound states are given by³⁹,

$$\varepsilon_n = \Delta_0 \sqrt{1 - T_n \sin^2(\phi/2)}, \quad n = 0, 1, 2, \dots \quad (15)$$

Using this result Eq. 11 for Josephson current is reduced to

$$I(\phi) = \frac{e\Delta_0}{\hbar} \sum_{n=0}^\infty \frac{T_n \sin \phi}{\sqrt{1 - T_n \sin^2(\phi/2)}} \varepsilon_n(\phi). \quad (16)$$

Further, the normal state resistance R_N is given by

$$1/R_N = \frac{4e^2}{\hbar} \sum_{n=0}^\infty T_n. \quad (17)$$

The normal state transmission probability T_n is calculated by a simple mode matching in the normal state structure³⁴. Using the wave function given by Eq. 5 for normal state and taking the limit of $U_0 \rightarrow \infty$ we can obtain the transmission probabilities as³⁴,

$$T_n = \frac{16}{\pi^2 (kR_1)(kR_2)} \frac{1}{(\Gamma_n^+)^2 + (\Gamma_n^-)^2}, \quad (18)$$

where

$$\Gamma_n^{+(-)} = \text{Im} \left[H_n^{(1)}(kR_1) H_{n(n+1)}^{(2)}(kR_2) \right. \\ \left. + (-) H_{n+1}^{(1)}(kR_1) H_{n+1(n)}^{(2)}(kR_2) \right], \quad (19)$$

with $k = \mu / \hbar v$ and $n = m - 1/2$. Now we have all requirements for calculating the Josephson current in Corbino Josephson junction. In the next section we will give the results for critical current in this junction.

III. RESULTS AND DISCUSSION

In this section, we present results for the critical current I_c in terms of the reduced chemical potential $k_F L = \mu L / \hbar v$, with $L = R_2 - R_1$, and ratios of the outer to inner radii of Corbino disk R_2/R_1 , at zero temperature. Fig. 2 shows the critical current in terms of the reduced chemical potential for different R_2/R_1 . Similar to the planar junction, critical current has an oscillatory behavior and increases by increasing $k_F L$. This oscillatory behavior is due to phase coherent interference of the electrons and holes that carry the supercurrent caused by the formation of a Fabry-Pérot cavity. Increasing R_2/R_1 results in decreasing of I_c in response to the junction length ($L = R_2 - R_1$) increment and critical current goes to have a linear dependence on $k_F L$ at high values of radii ratio R_2/R_1 . The graphene Corbino Josephson junction supports a nonzero minimal supercurrent at the zero doping identical to the planar graphene Josephson junctions. This behavior is caused by the evanescent modes which

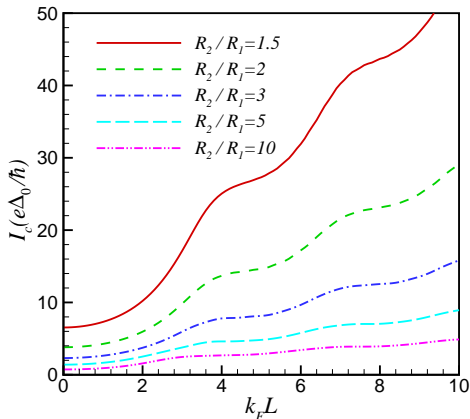


FIG. 2. (Color online) Critical Josephson current I_c of a Corbino Josephson junction as a function of the reduced chemical potential $k_F L$ for different values of R_2/R_1 .

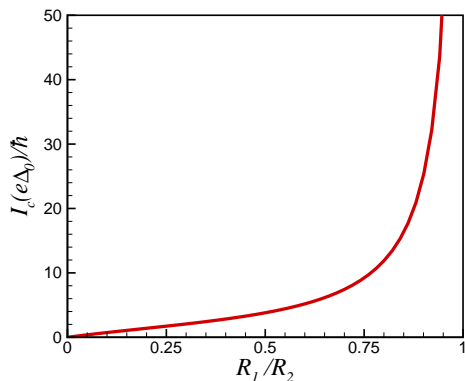


FIG. 3. (Color online) Critical Josephson current I_c of a Corbino Josephson junction as a function of radii aspect ratio of Corbino disk R_1/R_2 at zero doping.

are exist at the Dirac point in combination with the Klein tunneling effect. We have plotted the critical current in terms of R_1/R_2 in Fig. 3 to compare minimal supercurrent at zero doping for different values of the radii aspect ratio. This figure shows the scaling behavior of the critical current at zero doping. To analyze this nonzero minimal supercurrent we notice that at zero doping and in the limit of $R_2/R_1 \simeq 1$, the normal state conductivity of the Corbino junction scales by the factor $2\pi/Ln(R_2/R_1)^{34}$. In the opposite limit $R_2 \gg R_1$, conductance of the normal junction scales by $8\pi(R_1/R_2)$. Thus, as it is apparent in Fig. 3(a), the critical current takes a Logarithmic scaling when it approaches $R_1/R_2 = 1$, and it vanishes by increasing R_2/R_1 and tends linearly to zero in the limit of $R_1/R_2 \rightarrow 0$. The normalized critical Josephson current, $I_c Ln(R_2/R_1)/2\pi$, takes a constant value for $R_1/R_2 > 0.5$ as it has been shown in Fig. 4(a). Further, as Fig. 4(b) shows, the product of the critical Josephson

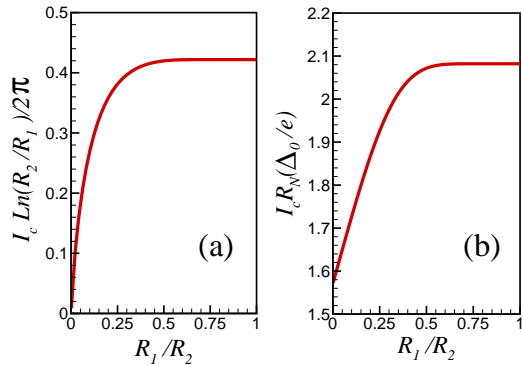


FIG. 4. (Color online) (a) Normalized critical Josephson current $I_c Ln(R_2/R_1)/2\pi$ and (b) product of the critical current and normal-state resistance as a function of radii aspect ratio of Corbino disk R_1/R_2 at zero doping.

current and normal-state resistance $I_c R_N$, approaches to its limiting value at $R_1/R_2 \rightarrow 1$ for $R_1/R_2 > 0.5$, and takes a nonzero value (~ 1.57) at the limit of $R_1/R_2 \rightarrow 0$. Since R_N has inverse scaling with respect to I_c , their product $I_c R_N$ takes nonzero value for all values of the R_1/R_2 at zero doping.

The limiting behavior of the critical current for $R_2/R_1 \rightarrow 1$ at zero doping can be deduced by investigating the limiting behavior of the transmission probability given by Eq. 18. At zero doping the transmission probability is given by³⁴,

$$T_j = \frac{1}{\cosh^2[j \ln(R_1/R_2)]}, \quad j = \frac{1}{2}, \frac{3}{2}, \frac{5}{2}, \dots \quad (20)$$

Then using Eq. 10 we can obtain the following expression for the Josephson current at zero doping and in the limit of $R_2/R_1 \rightarrow 1$,

$$\begin{aligned} I(\phi) &= \frac{e\Delta_0}{\hbar} \frac{4}{Ln(R_2/R_1)} \cos(\phi/2) \operatorname{arctanh}[\sin(\phi/2)], \\ I_c &= 1.33 \frac{e\Delta_0}{\hbar} \frac{2}{Ln(R_2/R_1)}, \\ I_c R_N &= 2.08 \frac{\Delta_0}{e}. \end{aligned} \quad (21)$$

These expressions match with the results presented in Figs. 3 and 4(a)(b). These results for ballistic graphene with Corbino geometry at the Dirac point are similar to those of a planar junction of a ballistic graphene or a disorder normal metal. Therefore, we revisit the pseudodiffusive behavior at zero doping for the graphene Corbino Josephson junction¹⁷.

To complete our discussion, the dependence of $I_c R_N$ on $k_F L$ for different values of R_2/R_1 has been depicted in Fig. 5. As these results show $I_c R_N$ reduces by increasing R_2/R_1 for all values of the carrier concentration. At the zero doping and in the limit of $R_2/R_1 \rightarrow 1$, $I_c R_N$ is correctly given by Eq. 21. On the other

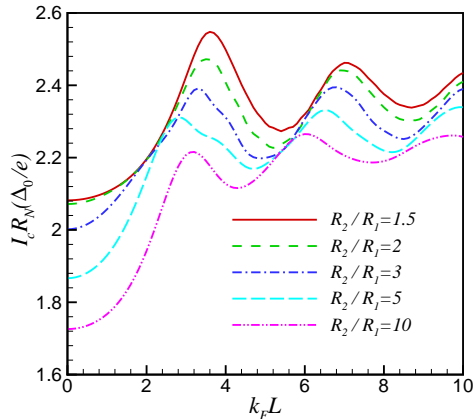


FIG. 5. (Color online) Product of the critical Josephson current and normal-state resistance $I_c R_N$ of a Corbino Josephson junction as a function of the reduced chemical potential $k_F L$ for different values of R_2/R_1 .

hand, at the limit of $k_F L \gg 1$ it approaches to the value given by $I_c R_N = 2.44\Delta_0/e$ identical to the planar graphene Josephson junctions. Recent realization of the ballistic graphene Josephson junctions with well defined superconductor and graphene contacts²⁹ and the resistance measurements performed on the graphene Corbino junction³³ makes it possible to observe the scaling behavior of the graphene Corbino Josephson junction reported here.

IV. CONCLUSIONS

In conclusion we have studied the Josephson current in the graphene Corbino Josephson junction. The Corbino Josephson junction has composed of a ring shape graphene attached to two coaxial superconducting leads. We have analyzed the Josephson current in the short junction limit by calculating the Andreev bound state energies. We have shown that the ballistic Corbino Josephson junction supports a nonzero critical Josephson current at the zero doping and behave similar to the diffusive Corbino Josephson junctions in the zero doping limit. This result revealed the pseudodiffusive behavior of the Corbino Josephson junction at zero doping identical to the planar junction. The critical Josephson current decreases monotonically by increasing the outer to inner radii ratio of Corbino junction. Moreover, we have shown that the product of the critical current and the normal-state resistance have a nonzero value for all values of the aspect ratios of radii of Corbino disk. The scaling behavior studied here can be observed in the experiment.

REFERENCES

- ¹B. D. Josephson, Phys. Lett. **1**, 251 (1962).
- ²K.K. Likharev, Rev. Mod. Phys. **51**, 101, (1979).
- ³A. F. Andreev, Sov. Phys. JETP **19**, 1228 (1964).
- ⁴Y. Makhlin, G. Schön, A. Shnirman, Rev. Mod. Phys., **73**, 357-400 (2001).
- ⁵J. Clarke, and F. K. Wilhelm, Nature **453**, 1031-1042 (2008).
- ⁶Yu. A. Pashkin, T. Yamamoto, O. Astafiev, Y. Nakamura, D. V. Averin, and J. S. Tsai, Nature **421**, 823 (2003).
- ⁷H. Mooij, Science **307**, 1210 (2005).
- ⁸K. G. Fedorov, A. V. Shcherbakova, R. Schäfer, and A. V. Ustinov, Appl. Phys. Lett. **102**, 132602 (2013).
- ⁹K. G. Fedorov, A. V. Shcherbakova, M. J. Wolf, D. Beckmann, and A. V. Ustinov, Phys. Rev. Lett. **112**, 160502 (2014).
- ¹⁰K.S. Novoselov, A.K. Geim, S.V. Morozov, D. Jiang, Y. Zhang, S.V. Dubonos, I.V. Grigorieva, and A.A. Firsov, Science **306**, 666 (2004).
- ¹¹K.S. Novoselov, A.K. Geim, S.V. Morozov, D. Jiang, M.I. Katsnelson, I.V. Grigorieva, S.V. Dubonos, A.A. Firsov, Nature **438**, 197 (2005).
- ¹²A. K. Geim and K. S. Novoselov, Nature Mat. **6**, 183 (2007).
- ¹³M. I. Katsnelson and K. S. Novoselov, Solid State Comm. **143**, 3 (2007).
- ¹⁴T. Ando, J. Phys. Soc. Jpn. **74**, 777 (2005).
- ¹⁵C. W. J. Beenakker, Phys. Rev. Lett. **97**, 067007 (2006).
- ¹⁶C. W. J. Beenakker, Rev. Mod. Phys. **80**, 1337 (2008)
- ¹⁷M. Titov and C. W. J. Beenakker, Phys. Rev. B **74**, 041401(R) (2006).
- ¹⁸Ali G. Moghaddam, Malek Zareyan, Phys. Rev. B **74**, 241403(R) (2006).
- ¹⁹Ali G. Moghaddam, Malek Zareyan, Appl. Phys. A **89**, 579-585 (2007).
- ²⁰I. Hagymási, A. Kormányos, and József Cserti, Phys. Rev. B **82**, 134516 (2010).
- ²¹A. M. Black-Schaffer and S. Doniach, Phys. Rev. B **78**, 024504 (2008).
- ²²A. M. Black-Schaffer and J. Linder, Phys. Rev. B **82**, 184522 (2010).
- ²³M. Alidoust and J. Linder, Phys. Rev. B **84**, 035407 (2011).
- ²⁴J. Gonzalez, and E. Perfetto, J. Phys.: Condens. Matter **20**, 145218 (2008).
- ²⁵H. B. Heersche, P. Jarillo-Herrero, J. B. Oostinga, L. M. K. Vandersypen and A. F. Morpurgo, Nature **446**, 56-59 (2007).
- ²⁶F. Miao, S. Wijeratne, Y. Zhang, et.al., Science **317**, 1530 (2007).
- ²⁷A. Shailos, W. Nativel, A. Kasumov, et.al., EPL **79**, 57008 (2007).
- ²⁸Xu Du, Ivan Skachko, and Eva Y. Andrei, Phys. Rev. B **77**, 184507 (2008).
- ²⁹V. E. Calado, S. Goswami, G. Nanda, M. Diez, A. R. Akhmerov, K. Watanabe, T. Taniguchi, T. M. Klapwijk, and L. M. K. Vandersypen, Nature Nanotechnology **10**, 761764 (2015).
- ³⁰C. D. English, D. R. Hamilton, C. Chialvo, I. C. Moraru, N. Mason, and D. J. Van Harlingen, Phys. Rev. B **94**, 115435 (2016).
- ³¹C.W.J. Beenakker, H. van Houten, Phys. Rev. Lett. **66**, 3056 (1991).
- ³²R. H. Hadfield, G. Burnell, Dae-Joon Kang, C. Bell, and M. G. Blamire, Phys. Rev. B **67**, 144513 (2003).
- ³³J. Yan and M. S. Fuhrer, Nano Lett. **10**, 45214525 (2010).
- ³⁴A. Rycerz, P. Recher, and M. Wimmer, Phys. Rev. B **80**, 125417 (2009).
- ³⁵A. Rycerz, Phys. Rev. B **81** 121404(R) (2010).
- ³⁶B. Abdollahipour, E. Moomivand, Physica E **86**, 204-209 (2017).
- ³⁷József Cserti and Imre Hagymási, Phys. Rev. B **80**, 073404 (2009).
- ³⁸P. Recher, B. Trauzettel, A. Rycerz, Ya. M. Blanter, C. W. J. Beenakker, and A. F. Morpurgo, Phys. Rev. B **76**, 235404 (2007).
- ³⁹C.W.J. Beenakker, Phys. Rev. Lett. **67**, 3836 (1991).